



Multilayer hybrid nanosheet of mesoporous carbon – layered metal oxide as a highly efficient electrocatalyst for Li – O₂ batteries

Yun Kyung Jo^{a,1}, Wilson Tamakloe^{b,1}, Xiaoyan Jin^a, Joohyun Lim^a, Sharad B. Patil^a, Yong-Mook Kang^{b,*}, Seong-Ju Hwang^{a,*}

^a Center for Hybrid Interfacial Chemical Structure (CICS), Department of Chemistry and Nanoscience, College of Natural Sciences, Ewha Womans University, Seoul 03760, Republic of Korea

^b Department of Energy and Materials Engineering, Dongguk University-Seoul, Seoul 04620, Republic of Korea



ARTICLE INFO

Keywords:

Electrocatalyst
Li-O₂batteries
Manganese oxide
Mesoporous carbon
Multilayer hybrid 2D nanosheet

ABSTRACT

An effective methodology to explore highly efficient oxygen electrocatalysts and electrodes for Li – O₂ batteries is developed via intimate layer-by-layer hybridization between mesoporous carbon layer and highly anisotropic 2D metal oxide nanosheets. The obtained multilayer hybrid nanosheets of mesoporous carbon – layered MnO₂ display outstanding functionalities as oxygen electrocatalysts with low overpotential and as the electrodes of Li – O₂ batteries with huge discharge capacity of ~7000 mAhg⁻¹ at 200 mA g⁻¹ and improved cyclability. The excellent electrocatalyst/electrode bifunctionality of the present material is attributable to enhanced electron transfer kinetics, maximized active sites, promoted electrocatalysis kinetics, and stabilization of unstable Mn³⁺ species. This multilayer hybrid nanosheet structure is advantageous for facilitating reversible formation/decomposition of discharged product during cycling in Li – O₂ batteries via promoted electrolyte – oxygen diffusion. The present study underscores that exfoliated metal oxide nanosheet can be used as an efficient immobilization matrix for synthesizing novel 2D multilayer hybrid nanosheets with synergistically-improved electrocatalyst/electrode functionalities.

1. Introduction

The exploration of economically-feasible high-performance electrocatalysts is of crucial importance in emerging energy conversion technologies such as water electrolysis, fuel cell, and metal – O₂ batteries [1–3]. A great deal of research effort has been devoted for synthesizing cost-effective transition-metal-oxide-based electrocatalysts to replace conventional noble-metal-based ones [4,5,6,7]. The hybridization of nanostructured metal oxide with other species can provide a powerful methodology to optimize its electrocatalyst performance [8–10]. To date, most of hybrid materials are synthesized by the anchoring of electrocatalyst crystals on the surface of conductive materials such as graphene [8–10]. Since the beneficial effect of hybridization originates from the electronic coupling between hybridized species, the interfacial electronic interaction should be maximized for the optimization of the electrocatalyst performance of hybrid materials [11–18]. As building blocks for hybrid electrocatalysts, exfoliated inorganic nanosheets like transition metal oxide are highly promising because of their unusually high surface-to-volume ratio, well-defined

surface structure and wide bifacial surface, which is beneficial for enhancing the interfacial electronic coupling of nano-hybrid [17,18]. However, it is difficult to fabricate precisely-matched and well-defined interfaces between layered metal oxide nanosheets and hybridized species. To circumvent this difficulty, layer-by-layer hybridization of transition metal oxide nanosheet with other species is supposed to provide a highly effective way of exploring high-performance functional materials, since the atomic-level contact between layer-by-layer-stacked components induces unusually strong interfacial electronic coupling between them. One of the most promising candidates for secondary layers on metal oxide nanosheet is mesoporous carbon [19], because the uniform deposition of thin mesoporous carbon layer on electrocatalytically-active metal oxide nanosheet enables to synthesize unique multilayer hybrid nanosheets with optimized pore structure and improved functionalities. Also, the intimate interfacial interaction in the multilayer hybrid nanosheet allows to tailor the bonding nature of core metal oxide nanosheet. This layer-by-layer hybridization strategy can provide an effective way of developing economically-feasible transition-metal/carbon-based electrocatalysts for replacing

* Corresponding authors.

E-mail addresses: dake1234@dongguk.ac.kr (Y.-M. Kang), hwangsj@ewha.ac.kr (S.-J. Hwang).

¹ These authors contributed equally to this work.

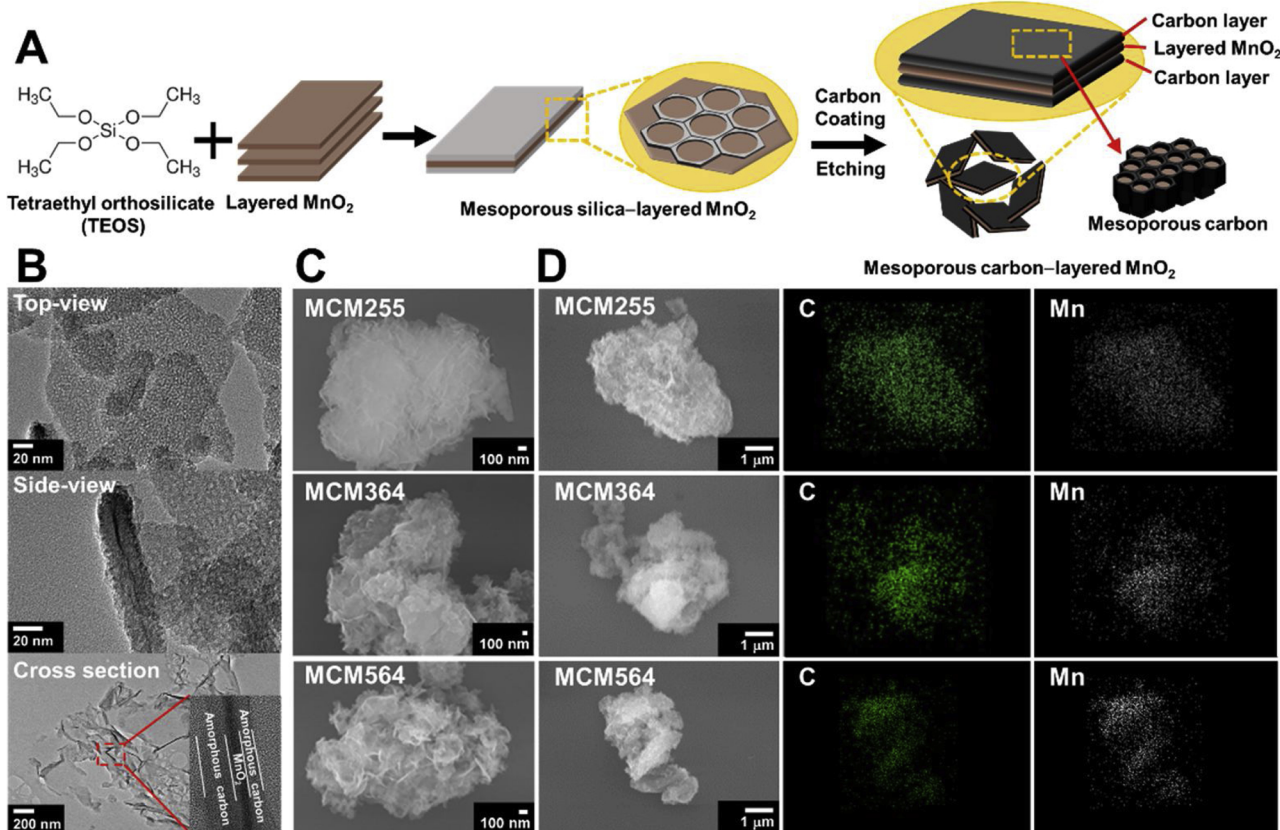


Fig. 1. (A) Schematic illustration of synthetic route, (B) TEM images of MCM564. (C) FE-SEM and (D) EDS – elemental maps of MCM.

conventional noble-metal-based ones. Despite unique advantages of multilayered hybrid nanosheet morphology, at the time of this submission, we are unaware of any other reports about the synthesis of 2D multilayer hybrid nanosheet of mesoporous carbon–layered metal oxide.

In this study, we report for the first time a novel effective methodology to synthesize the unprecedented multilayered hybrid nanosheets of transition metal oxide–mesoporous carbon, in which open-channels in mesoporous carbon are oriented perpendicularly to the surface of layered metal oxide nanosheets with well-defined interfaces. The 2D multilayer hybrid nanosheets of mesoporous carbon–layered MnO_2 (δ - MnO_2) are synthesized by the uniform coating of mesoporous carbon layer on the bifacial 2D surface of exfoliated MnO_2 nanosheet using silica template, as illustrated in Fig. 1A. The present multilayer 2D–2D layered δ - MnO_2 –carbon hybrid nanosheets show an outstanding electrocatalyst performance for Li–O₂ battery, which is superior to the other MnO_2 –carbon based hybrid materials including α - MnO_2 -containing ones, as summarized in Table S1 of Supporting Information. The remarkable usefulness of the present heterolayer hybridization strategy in exploring efficient functional materials is obviously evidenced by excellent performances of multilayer 2D–2D hybrid nanosheets as oxygen electrocatalysts and electrodes for Li–O₂ batteries.

2. Experimental

2.1. Synthetic procedures

As precursors for 2D multilayer hybrid nanosheets of carbon–layered MnO_2 , mesoporous silica–layered MnO_2 hybrid nanosheets were synthesized by deposition of mesoporous silica layers on the surface of exfoliated MnO_2 nanosheet using tetraethyl orthosilicate (TEOS). The carbon coating for the obtained precursor nanosheet was achieved by the following multistep process [20,21]; first, Al^{3+} ion

was doped for the mesopore wall of the 2D silica–layered MnO_2 hybrid nanosheet. The obtained Al^{3+} -doped precursor materials were dispersed in mesitylene with phenol and paraformaldehyde. The restored powdery mixtures were heated at 90 °C for 12 h, and then heated at 800 °C for 3 h under Ar flow, leading to the formation of mesoporous carbon layer on the surface of layered MnO_2 nanosheet. The alkaline etching for the silica layer yielded 2D multilayer hybrid nanosheets of mesoporous carbon–layered MnO_2 (denoted as MCM hybrid nanosheets). To control the carbon/ MnO_2 ratio in the MCM hybrid nanosheet, several amounts of TEOS solution (255, 364, and 564 μL) were employed for the synthesis of the precursor silica-containing hybrid nanosheets. The obtained multilayer hybrid 2D nanosheets of mesoporous carbon–layered MnO_2 were denoted as MCM255, MCM364, and MCM564, respectively. The controllability of carbon content in MCM nanosheets with the change of TEOS concentration was confirmed by thermogravimetric analysis (TGA), see Fig. S1 of Supporting Information. To study the effect of layer-by-layer hybridization on functionalities, two kinds of 0D and 2D mesoporous carbon materials were prepared as references. Mesoporous 2D carbon (denoted as MC564, see Fig. S2 of Supporting Information) was prepared by the acidic etching of MnO_2 component from MCM564 via the soaking in 5 M HCl aqueous solution at 60 °C for 24 h. Another reference of mesoporous 0D carbon nanosphere (denoted as MC) was synthesized by the identical synthetic process except for the absence of MnO_2 nanosheet, in which mesoporous silica nanoparticles were prepared and thus used as the precursor for MC. Field emission-scanning electron microscopy (FE-SEM) and transmission electron microscopy (TEM) analyses for both and mesoporous silica and MC nanoparticles clearly demonstrated the maintenance of monodisperse 0D spherical morphology with narrow size distribution of ~40–50 nm before and after carbonization at elevated temperature, see Fig. S3 of Supporting Information. The transformation from mesoporous silica to mesoporous carbon was further confirmed by

powder X-ray diffraction (XRD) and N_2 adsorption–desorption isotherm analyses (Fig. S3).

2.2. Electrochemical measurement

The electrocatalytic activity was investigated by linear sweep voltammetry (LSV) method using three-electrode glass cell with a scan rate of 10 mV s^{-1} in O_2 -saturated 0.1 M KOH aqueous solution. Before the measurement, oxygen gas was bubbled into the electrolyte for 30 min. The LSV curves carried out by RRDE-3A (ALS Co.) as a rotator and an IVIUM analyzer with a three-electrode cell. The rotating ring-disk electrode (RRDE) voltammograms were measured using the three-electrode cell with a bi-potentiostat. The ring current was measured on the Pt-ring glassy carbon disk electrode (ALS Co.) at a scan rate of 10 mV s^{-1} with a ring potential of 1.3 V . The electrochemical impedance spectroscopy (EIS) data were collected with IVIUM analyzer in the frequency region of $0.01\text{--}30000\text{ Hz}$ at -0.067 V (V vs. SHE). Electrochemical tests were undertaken using a Swagelok-type $\text{Li} - \text{O}_2$ cell system with lithium metal as anode, Whatman micro-glass fiber as separator and electrodes prepared with active materials (**MCM**, **MC564**, and layered MnO_2) as cathodes. For the test of $\text{Li} - \text{O}_2$ electrode activity, 1 M lithium triflate in TEGDME was used as the electrolyte instead of 0.1 M KOH solution employed for ORR activity test, because aqueous electrolytes tend to be volatile during cycling of $\text{Li} - \text{O}_2$ battery cell [22]. Conversely, TEGDME was reported to enhance the cyclability of $\text{Li} - \text{O}_2$ cell by the suppression of solvent evaporation, which merits the use of this electrolyte [22]. Cyclic voltammetry (CV) measurements were carried out at 5 mV s^{-1} for each cell between $2\text{--}4.5\text{ V}$ and the corresponding current (mA)–voltage (V) data were plotted. Galvanostatic charge–discharge (CD) tests were performed using Wonatech Land Cyclers at voltage cut-offs of 2.0 (lower limit) and 4.5 V (upper limit). The application of a wide potential range for galvanostatic CD measurement of $\text{Li} - \text{O}_2$ cell prevented from employing aqueous KOH electrolyte due to its narrow potential window. Instead, TEGDME having wide potential window made this electrolyte proper for the test of $\text{Li} - \text{O}_2$ electrode activity. Cycle life measurements were conducted at limited discharge–charge under constant-current constant–voltage at capacity cut-off of 1000 mA h g^{-1} of the active material. EIS analysis for $\text{Li} - \text{O}_2$ cells was also carried out within the frequency range of $10\text{ kHz} - 100\text{ MHz}$ at a 10 mV AC voltage amplitude on an IVIUM Electrochemical Workstation. Experimental details for synthetic procedures and characterizations are provided in Supporting Information.

3. Results and discussion

The formation of multilayer structure composed of core MnO_2 nanosheet and hexagonally-ordered mesoporous carbon coating layers is verified by TEM analysis (Fig. 1B). The distinct morphological difference between **MCM** and **MC** is regarded as another evidence for the successful surface anchoring of uniform 2D carbon layer on MnO_2 nanosheet (Fig. S3 of Supporting Information). As shown in Fig. 1C, FE-SEM analysis clearly demonstrates the house-of-cards-type stacking structures of **MCM**, confirming the maintenance of 2D nanosheet morphology and porous structure upon the formation of multilayer hybrid nanosheet. The homogeneous immobilization of mesoporous carbon layer on the MnO_2 nanosheet is further confirmed by energy dispersive spectrometry (EDS)–elemental mapping analysis showing the uniform distribution of Mn and C elements in the entire part of **MCM**, see Fig. 1D. As plotted in the powder XRD patterns of Fig. S4 of Supporting Information, all the **MCM** hybrid nanosheets commonly display an intense and broad feature at $2\theta = \sim 1^\circ$ corresponding to the (100) reflection of hexagonally-ordered mesoporous carbon phase, indicating the presence of mesoporous carbon layer in these hybrid materials [23]. Additionally, a distinct diffraction peak corresponding to the (002) reflection of carbon species is discernible at $2\theta = \sim 26^\circ$ for all the present materials [24]. The observed XRD features of **MCM**

nanohybrids are nearly identical to those of the mesoporous carbon references (**MC** and **MC564**) (Fig. S4 of Supporting Information), providing convincing evidence for the formation of mesoporous carbon layers in the **MCM** hybrid nanosheets. Conversely, there are no layered MnO_2 -related Bragg reflections in the present XRD patterns of the **MCM** hybrid nanosheets, strongly suggesting the homogeneous dispersion of monolayered MnO_2 nanosheet without phase segregation. The hybridization between carbon and MnO_2 is further confirmed by micro-Raman results showing characteristic spectral features of both species, see Fig. S5 of Supporting Information. According to C 1s X-ray photo-electron spectroscopy (XPS) data in Fig. S6 of Supporting Information, all the **MCM** hybrid nanosheets display nearly identical carbon-related components centered at ~ 284.7 , ~ 285.2 , ~ 287.0 , and $\sim 288.9\text{ eV}$, which are assigned as C–C, C–O, C=O, and carboxyl species, respectively [25]. This result confirms the deposition of carbon layer with similar bonding nature in these hybrid materials. In contrast to **MCM**, **MC** shows additional higher-energy component at $\sim 290\text{ eV}$ corresponding to $\pi - \pi^*$ transition, reflecting intramolecular charge transfer of carbon species [26]. The significant depression of this peak for **MCM** suggests the lowering of π electron density due to the interfacial charge transfer between carbon and MnO_2 . As presented in Fig. S6 and Table S2 of Supporting Information, the peak deconvolution analysis for Mn 2p XPS data demonstrates that an increase of carbon amount in **MCM** enhances Mn^{3+} content with the lowering of average Mn oxidation state. This is attributable to the partial oxygen loss of MnO_2 during the combustion of organic precursor.

The revolution of Mn oxidation state and local structure upon hybridization is further evidenced by Mn K-edge extended X-ray absorption fine structure (EXAFS) analysis. As depicted in Fig. 2, all the **MCM** hybrid nanosheets commonly show two intense FT peaks corresponding to $(\text{Mn} - \text{O})$ and $(\text{Mn} - \text{Mn})$ coordination shells at ~ 1.5 and $\sim 2.6\text{ \AA}$, respectively, indicating the maintenance of layered $\delta\text{-MnO}_2$ lattice consisting of edge-shared MnO_6 octahedra. A closer inspection reveals that the anchoring of mesoporous carbon layer depresses the first FT peak, reflecting the increase of local structural disorder caused by the increase of Jahn-Teller-active Mn^{3+} ion [27]. Since both equatorial $(\text{Mn}^{3+} - \text{O}_{\text{eq}})$ and $(\text{Mn}^{4+} - \text{O})$ shells possess nearly identical bond distances of $\sim 1.9\text{ \AA}$ and axial $(\text{Mn}^{3+} - \text{O}_{\text{ax}})$ shell has longer bond distance of $\sim 2.3\text{ \AA}$ [27], the EXAFS curve-fitting analysis is carried out with structural model composed of two different $(\text{Mn} - \text{O})$ bonding shells. In one instance, mixed manganese oxide (e.g. $\text{MnO}_{1.75}$) with average Mn oxidation state of $+3.5$ (i.e. $[\text{Mn}^{3+}] / [\text{Mn}^{4+}] = 1$) possesses the $(\text{Mn}^{4+} - \text{O} / \text{Mn}^{3+} - \text{O}_{\text{eq}})$ and $(\text{Mn}^{3+} - \text{O}_{\text{ax}})$ bonds in the ratio of 5:1. The variation of the ratio of these bonds can provide quantitative information about the average Mn oxidation state of the present **MCM** hybrid nanosheets. Due to the strong correlation between coordination number (CN) and Debye–Waller factor (σ^2), the σ^2 values are set the same for two kinds of $(\text{Mn} - \text{O})$ shells to probe the variation of their CN values upon the change of carbon content. Based on this structural model, the experimental FT spectra of **MCM** nanosheets as well as layered MnO_2 are well-reproduced, as plotted in Fig. 2. As summarized in Table 1, an increase of carbon content increases coordination number (CN) for $(\text{Mn}^{3+} - \text{O}_{\text{ax}})$ bonds, confirming a gradual increase of Mn^{3+} content. Since Mn^{3+} species with e_g^1 electronic configuration plays a crucial role in oxygen reduction reaction (ORR) [28], the increase of Mn^{3+} content strongly suggests the beneficial effect of layer-by-layer hybridization on electrocatalytic activity.

As plotted N_2 adsorption–desorption isotherm data in Fig. S7 of Supporting Information, all the present materials exhibit distinct N_2 adsorption with distinct hysteresis, indicating their significant porosity. The Brunauer–Emmett–Teller surface areas of the present materials are determined as $586\text{ m}^2\text{ g}^{-1}$ for **MCM255**, $745\text{ m}^2\text{ g}^{-1}$ for **MCM364**, $1044\text{ m}^2\text{ g}^{-1}$ for **MCM564**, $1040\text{ m}^2\text{ g}^{-1}$ for **MC**, $821\text{ m}^2\text{ g}^{-1}$ for **MC564**, and $12\text{ m}^2\text{ g}^{-1}$ for layered MnO_2 , respectively. Of noteworthy is that, despite its lower carbon content, **MCM564** shows a larger surface area than do the mesoporous carbon references (**MC** and **MC564**),

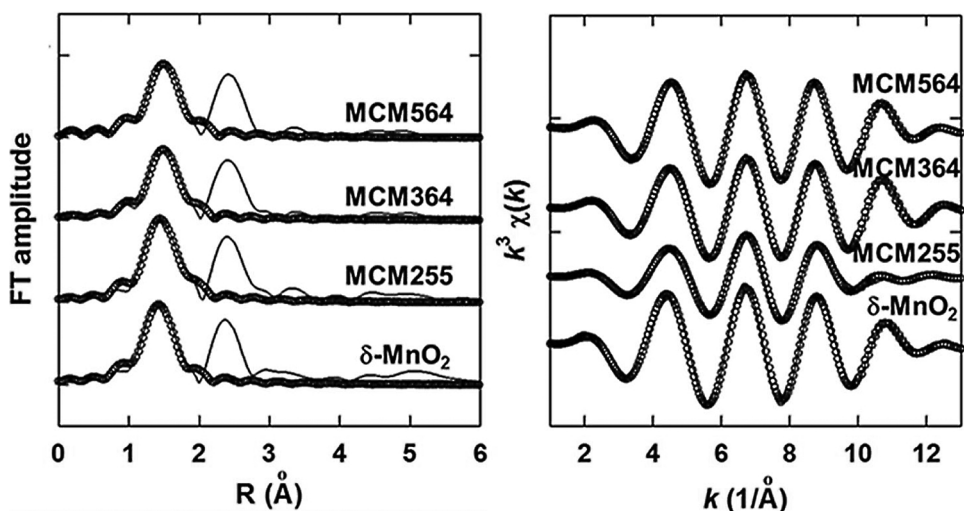


Fig. 2. (Left) Fourier transformed (FT) data and (right) inverse FT data of Mn K-edge EXAFS spectra of the MCM hybrid nanosheets and layered MnO₂ with the best fits. The solid lines and circles represent the experimental and fitted data, respectively.

Table 1

Results of nonlinear least-squares curve fittings for the first peak of Mn K-edge EXAFS spectra of the layered MnO₂ and MCM nanosheets.

Sample	Bond	CN	R (Å)	$\Sigma^2(10^{-3} \text{ Å}^2)$
Layered MnO ₂	(Mn ⁴⁺ –O/Mn ³⁺ –O _{eq})	5.41	1.88	3.27
	(Mn ³⁺ –O _{ax})	0.59	2.23	3.27
MCM255	(Mn ⁴⁺ –O/Mn ³⁺ –O _{eq})	4.92	1.89	2.60
	(Mn ³⁺ –O _{ax})	1.08	2.24	2.60
MCM364	(Mn ⁴⁺ –O/Mn ³⁺ –O _{eq})	4.81	1.91	2.80
	(Mn ³⁺ –O _{ax})	1.19	2.26	2.80
MCM564	(Mn ⁴⁺ –O/Mn ³⁺ –O _{eq})	4.74	1.92	3.39
	(Mn ³⁺ –O _{ax})	1.26	2.27	3.39

The curve fitting analysis was performed for the range of $2.700 - k - 11.300 \text{ Å}^{-1}$ and $0.644 - R - 2.056 \text{ Å}$.

underscoring the beneficial effect of layer-by-layer hybridization with MnO₂ nanosheet on porosity by preventing the self-stacking upon the $\pi - \pi^*$ interaction between mesoporous carbon layers. This result is cross-confirmed by pore volume calculation exhibiting a larger pore volume of MCM564 ($1.54 \text{ cm}^3 \text{ g}^{-1}$) than those of MC ($1.25 \text{ cm}^3 \text{ g}^{-1}$) and MC564 ($0.74 \text{ cm}^3 \text{ g}^{-1}$), emphasizing the enhancement of porosity caused by the non-aggregated deposition of mesoporous carbon layers on the surface of MnO₂ nanosheet. Such enhancement of porosity upon layer-by-layer hybridization is beneficial for improving the oxygen electrocatalyst performance via the provision of more oxygen adsorption sites and the improved diffusion of electrolyte and oxygen [29].

To investigate the effect of multilayer hybridization on the electrocatalyst performance, the MCM hybrid nanosheets as well as 2D mesoporous carbon (i.e. MC564) and layered MnO₂ are applied as electrocatalysts for ORR in alkaline condition. As shown in LSV curves of Figs. 3A and S8 of Supporting Information, all the MCM materials display superior ORR electrocatalytic performances with much more positive half-wave potentials than do MC564 and layered MnO₂, underscoring the merit of layer-by-layer hybridization on electrocatalyst performance. The interstratification of alternating MnO₂ layer and mesoporous carbon layer can prevent agglomeration of each 2D component during electrocatalytic reaction due to the depression of hydrophilic interaction between MnO₂ nanosheets and $\pi - \pi^*$ interaction between carbon layers. The resulting suppression of the tight stacking of MnO₂ nanosheets and carbon species is quite effective in maintaining the expanded surface area and catalytically active surface sites of multilayer hybrid MCM nanosheet during the electrocatalytic reaction, which is responsible for the beneficial effect of multilayer hybridization

[30,31]. Additionally, as evidenced by XPS and EXAFS analysis, the occurrence of partial oxygen loss in tetravalent MnO₂ nanosheet during the combustion of organic precursor increases the content of reduced Mn³⁺ ion. Since the increase of Mn³⁺ ion enhances an electron transfer with adsorbed oxygen species and thus the ORR kinetics of manganese oxide [28], the stabilization of this species by the oxygen loss can make additional contribution to the improved electrocatalytic activity of the present MCM nanocomposites. Beyond an optimal ratio of MCM564, a further increase of carbon content leads to the degrading of ORR activity (Fig. S9 of Supporting Information), strongly suggesting the significant contribution of both MnO₂ and carbon components to the improved electrocatalyst performance of MCM. From the Koutecky–Levich (K–L) plots of Fig. 3C, MCM564 shows a much larger electron transfer number (n) of 3.94 than that of MC564 (2.71), highlighting the usefulness of multilayer hybridization in improving ORR kinetics toward four-electron transfer pathway. The positive effect of layer-by-layer structure on ORR kinetics is further evidenced by much lower production HO₂[–] yield (~2%) and lower Tafel slope of MCM564 (96 mV dec^{–1}) than those of MC564 (~4% and 126 mV dec^{–1}), see Fig. 3E and 3F. The observed improvement of ORR kinetics is attributable to the optimized pore structure, surface area, and enhanced interfacial interaction [32]. The MCM564 shows better long-term durability with ~86% retention after 20,000 s, which is better than that of MC564 (~83%). Since the electrochemical stability of carbon species is strongly dependent on the maintenance of porous stacked structure and expanded surface area during the electrocatalytic reaction, the improved electrocatalytic durability of MCM hybrid nanosheets is attributable to the increased stability of mesoporous carbon layers caused by the intervention of MnO₂ nanosheet, resulting in the depression of $\pi - \pi^*$ interaction between carbon layers. This result emphasizes the beneficial role of multilayered hybrid structure in improving electrochemical stability. As illustrated in Fig. 3H, the MCM564 exhibits negligible current decay after the injection of methanol, which is in stark contrast to MC564 showing notable current depression, indicating the improvement of selectivity toward ORR upon the formation of multilayer hybrid structure. This finding clearly demonstrates that intervention of MnO₂ nanosheet between mesoporous carbon layers is effective in depressing the serious methanol crossover of mesoporous carbon species via the prevention of severe frustration in the presence of methanol.

To further verify the effect of multilayer hybridization on electrocatalyst performance, the physical mixture of mesoporous carbon and layered MnO₂ with the same composition as that of MCM564 (denoted as PMCM564) is also tested as ORR electrocatalyst. As plotted in

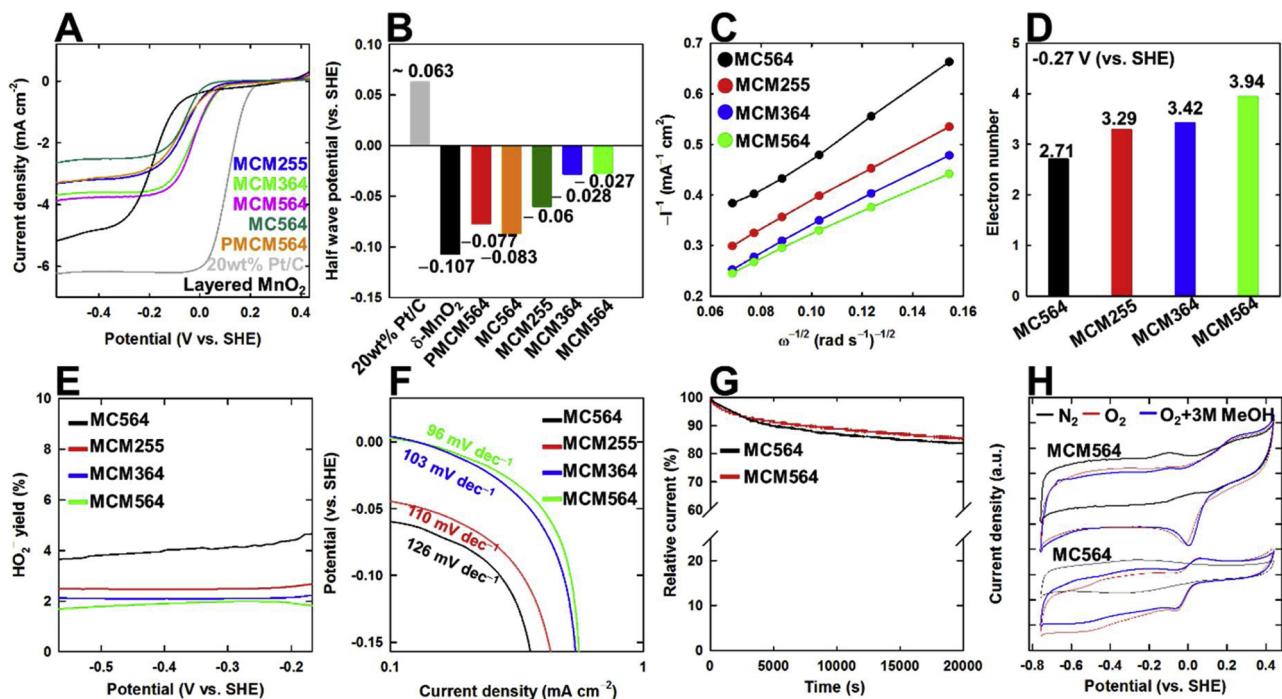


Fig. 3. (A) LSV plots and (B) half-wave potentials for MCM, MC564, layered MnO₂, PMCM564, and 20 wt% Pt/C. (C) K–L plots, (D) electron transfer number plots, (E) peroxide yield plots, (F) Tafel plots, (G) ORR durability data, and (H) CV curves of methanol tolerance test for MCM and MC564.

Fig. 3A, the electrocatalyst performance of **PMCM564** is much poorer than that of **MCM564**, confirming the beneficial influence of intimate layer-by-layer hybridization and the contribution of MnO₂ nanosheet to the improved functionality. Additionally, the hybrid material of 2D MnO₂ nanosheet and 0D mesoporous carbon nanoparticle (MC) is also synthesized as a reference and employed as ORR electrocatalyst to confirm the advantage of 2D–2D multilayer hybrid nanosheets in optimizing the oxygen electrocatalyst performance. In comparison with the present 2D–2D MnO₂–carbon hybrid nanosheet of **MCM564**, the 2D–0D MnO₂ nanosheet–mesoporous carbon nanoparticle hybrid material delivers much inferior electrocatalyst performance (Fig. S10 of Supporting Information), underscoring the unique advantage of multilayer 2D–2D hybrid architecture in optimizing the electrocatalyst functionality of carbon and metal oxide. This result provides strong evidence for the novelty of the present multilayer hybridization strategy as a powerful synthetic route to explore efficient electrocatalyst materials.

As shown in electrochemical impedance data of Fig. S11 and Table S3 of Supporting Information, **MCM564** displays smaller semicircle corresponding to the charge transfer resistance (R_{ct}) and larger capacitance (C_{dl}) than does **MC564**, indicating the enhancement of electron transfer property and improved accessibility of oxygen species to the electrocatalytically active sites. Since a fast electron transfer from Mn³⁺ to adsorbed oxygen species plays an important role in the rate limiting step of ORR (Fig. S12 of Supporting Information), the enhancements of charge transfer kinetics and oxygen adsorptivity make additional crucial contribution to the improved ORR performance of **MCM**.

Based on its promising oxygen electrocatalytic activity, **MCM564** is employed as a cathode catalyst of Li–O₂ batteries, as compared with mesoporous 2D carbon (**MC564**) and layered MnO₂. As plotted in the CD curves (Fig. 4A), **MCM564** displays much greater discharge capacity (6932 mA h g⁻¹) at 200 mA g⁻¹ and smaller charging overpotential (1.38 V) than those of **MC564** (2584 mA h g⁻¹; 1.50 V) and layered MnO₂ (2035 mA h g⁻¹; 1.53 V). Also, much higher discharging potential occurs for **MCM564** than for the other materials. In CV curves of Fig. S13 of Supporting Information, a cathodic peak appears at a higher

onset potential of 2.50 V for **MCM564** than for **MC564** (2.25 V) and layered MnO₂ (2.20 V). The LSV curves of oxygen evolution reaction (OER) indicate much higher oxidative stability with a higher onset potential for **MCM564** (4.00 V) than for **MC564** (3.56 V) and layered MnO₂ (3.30 V) (Fig. 4B), underscoring the improved ORR and OER activities of hybrid nanosheet for Li–O₂ cathode. From the electrochemical test under CC–CV mode at limited capacity of 1000 mA h g⁻¹ (Fig. 4C), a very flat discharge plateau appears at 2.7 V commonly for **MCM564** and **MC564**, whereas layered MnO₂ shows a steep plateau. The **MCM564** exhibits a lower overpotential for charging and better cyclic retention than do **MC564** and layered MnO₂ (Fig. 4D). The present experimental findings underscore the crucial contribution of layered MnO₂ to the excellent electrocatalytic activity of the **MCM564** hybrid nanosheet. Of noteworthy is that, in contrast to **MCM564**, the layered MnO₂ shows drastically decreased cycle retention after the 3rd cycle. As plotted in Fig. S14A and S14B of Supporting Information, the XPS analysis clearly demonstrates that the discharge products of layered MnO₂ is formed after the ORR process and partially decomposed by the following OER process. This finding strongly suggests that the inefficient decomposition of discharge products during the CD process of layered MnO₂ leads to the surface deposition of thick insulating layer on the electrode and thus the significant blocking of oxygen gas pathway [33,34]. Such limited solubility and diffusivity of oxygen significantly degrades the cyclability of layered MnO₂ for Li–O₂ batteries. In comparison with layered MnO₂, the **MCM** hybrid nanosheet shows more efficient decomposition of the discharge products, indicating the beneficial effect of multilayer hybridization on charge transfer for dissociation of discharged products and the homogeneous formation/facile decomposition of discharge products at low overpotential. This is responsible for the promising cycle retention of multilayer hybrid **MCM564** nanosheet. As can be seen clearly from Fig. 4E and F, even at high current densities, the discharge capacities of **MCM564** are much larger than those of **MC564** and layered MnO₂. The crucial role of layer-by-layer hybridization between mesoporous carbon and MnO₂ is further confirmed by the inferior electrode performances of physically-mixed **PMCM564**, see Fig. S15 of Supporting Information. Such an excellent electrode performance of **MCM564** for Li–O₂

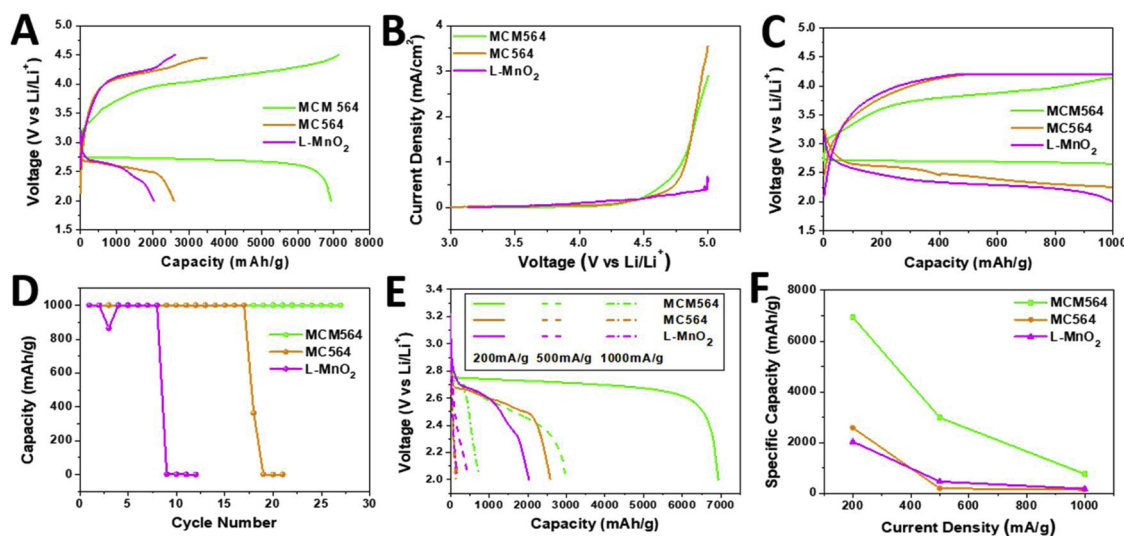


Fig. 4. (A) First CD curves, (B) LSV curves, (C) first CD curves in CC–CV mode at limited capacity of 1000 mA h g^{-1} , (D) cycle performances, (E) discharge capacity profiles at various current densities, and (F) current density-dependent discharge capacities for **MCM564**, **MC564**, and layered MnO_2 .

batteries is attributable to the enhancement of Li^+ ion diffusion and electron transfer originating from improved accessibility of oxygen species to the active sites. As an architectural reference for $\text{Li}-\text{O}_2$ electrode functionality, the 2D–0D MnO_2 nanosheet–mesoporous carbon nanoparticle hybrid material is compared with the optimized 2D–2D layered MnO_2 –mesoporous carbon nanosheet (**MCM564**) (see Fig. S16). The 2D–2D hybrid **MCM564** nanosheet delivers higher discharge capacity (6932 mA h g^{-1} at 200 mA g^{-1}) with an overpotential of 1.22 V at cut-off capacity of 1000 mA h g^{-1} , compared to that of 2D–0D nanohybrid (5124 mA h g^{-1} at 200 mA g^{-1}) with an overpotential of 1.49 V at 1000 mA h g^{-1} capacity cut-off. The relatively poorer performance of 2D–0D nanohybrid than 2D–2D homologue is attributable to the following two factors; (1) In contrast to layer-by-layer stacking structure of 2D MnO_2 nanosheet and 2D mesoporous carbon layer in **MCM564**, there is a significant variation in interfacial contacts between 2D MnO_2 nanosheet and 0D mesoporous carbon nanoparticle depending on their orientations, resulting in non-uniform surface activity. (2) The distance between 2D MnO_2 nanosheet and 0D mesoporous carbon varies depending on bond strength at the interface, impeding the interfacial charge transfer between carbon and manganese oxide. This comparative experiment provides strong evidence for remarkable advantage of 2D–2D multilayer hybridization strategy in exploring highly efficient electrocatalyst materials.

To date, there have been lots of researches about the hybrid materials composed of MnO_2 and carbon for the application as oxygen electrocatalysts and $\text{Li}-\text{O}_2$ cathodes, since these manganese oxide-based hybrid materials boast improved electrode/electrocatalyst performances and economical/environmental merits [35–50]. Among various polymorphs of MnO_2 , layered $\delta\text{-MnO}_2$ with numerous exposed catalytic active sites form an interconnected hierarchically porous structure with expanded basal spacing suitable for diffusion of oxygen and the immersion of electrolyte. In one instance, Zhang et al. reported a hybrid material of $\delta\text{-MnO}_2/\text{CCFs-K80}$ (carbon composite fibers) synthesized by the liquid deposition onto electrospun carbon fibers and its promising $\text{Li}-\text{O}_2$ electrode performance with a large capacity of 1076 mA h g^{-1} at 100 mA g^{-1} [35]. Liu et al. reported $\delta\text{-MnO}_2$ -based hybrid electrode via the direct growth of graphene and $\delta\text{-MnO}_2$ on Ni foam, which delivers a high discharge capacity of $\sim 3660 \text{ mA h g}^{-1}$ at 48 mA g^{-1} for $\text{Li}-\text{O}_2$ batteries [36]. The observed electrochemical performance of this material can be ascribed to its 3D scaffold structure allowing for facile oxygen diffusion and electrolyte immersion. Similarly, Wang et al. synthesized graphene-supported $\delta\text{-MnO}_2$ hybrid by using microwave-assisted growth method, which displays a

dramatically enhanced capacity (5862 mA h g^{-1} at 100 mA g^{-1}) for $\text{Li}-\text{O}_2$ cathode [37]. In comparison with these previous studies, the present multilayer 2D–2D hybrid **MCM564** nanosheet shows superior $\text{Li}-\text{O}_2$ cathode performance due to the its porous hybrid structure with expanded surface area and numerous active sites for the rapid diffusion of lithium ions and oxygen during battery cycling. Also, mesoporous carbon layer in this multilayer hybrid nanosheets forms a highly electrically conductive network, resulting in the improvement of electrical conductivity. It is worthwhile to mention that, despite the intrinsic inferior electrocatalyst performance of layered $\delta\text{-MnO}_2$ phase than $\alpha\text{-MnO}_2$ phase, the present multilayer 2D–2D **MCM564** nanohybrid exhibits much superior electrocatalyst functionality to the other MnO_2 -based nanohybrids including $\alpha\text{-MnO}_2$ -containing ones (Table S1), underscoring the outstanding validity of the present multilayer hybridization methodology in exploring efficient electrocatalyst materials.

The effects of CD cycling on the electrode morphologies and the nature of discharge product are further investigated with *ex-situ* FE-SEM and XPS analyses. As presented in Fig. S17 of Supporting Information, porous sheet-like discharge products are uniformly grown on the surface of **MCM564**, which is helpful to improve the diffusion of electrolyte and the nucleation of secondary discharge product [32]. After CD cycling, the discharge products of **MCM564** can be efficiently decomposed, which is in stark contrast to **MC564** and layered MnO_2 showing the incomplete decomposition of discharge products after recharging process. The observed fast decomposition of discharge products (Li_2O_2 , Li_2O , and carbonated-lithium species) is responsible for the improved electrode performance of **MCM564**, since the precipitation of discharge products on the surface of electrodes blocks the oxygen pathway and depresses the electrode performance. According to *ex-situ* $\text{Li} 1\text{s}$ XPS analysis (Fig. S14), **MCM564** exhibits the formation of discharge products after discharging and the remarkable depression of $\text{Li} 1\text{s}$ peak upon recharging process, indicating the efficient deposition/decomposition of discharge products on the surface of **MCM564**. In $\text{Mn} 2\text{p}$ XPS data (Fig. S14C and Table S4), **MCM564** experiences the lowering of Mn^{3+} content during discharging process due to the oxidation of Mn ion via ORR process [51], and the almost complete restoration of Mn^{3+} component upon recharging process, confirming the high reversibility of CD process in **MCM564**. Conversely, layered MnO_2 demonstrates less effective restoration of Mn^{3+} component during recharging process, which is attributable to a strong interaction between e_g orbitals of Mn^{3+} and 2p orbitals of reduced oxygen species. For **MCM564**, this interaction becomes weaker by the partial occupation of the e_g orbitals of Mn^{3+} by $\pi-\pi^*$ electrons from anchored carbon species, resulting in

the facilitation of OER. Although **MCM564** has a lower electrical conductivity than **MC564**, both the charged derivatives of **MCM564** and **MC564** show similar electrical conductivity (Fig. S18 of Supporting Information), emphasizing the complete decomposition of insulating discharge products in **MCM564** after charging process. Such effective complete decomposition of discharge products in **MCM564** can be ascribed to the role of uniform pores as tunnels to supply oxygen into the interior of electrode.

4. Conclusions

In this work, a novel effective methodology is developed for the first time to synthesize unprecedented multilayered 2D–2D hybrid nanosheets of transition metal oxide–mesoporous carbon via the layer-by-layer hybridization between layered metal oxide nanosheet and mesoporous carbon layer. The obtained hybrid nanosheets display outstanding performances as high-performance oxygen electrocatalysts for Li–O₂ electrode with remarkably improved discharge capacity and cyclability, highlighting the remarkable validity of the present methodology firstly reported in this work. As summarized in Table S1 of Supporting Information, despite the intrinsic inferior electrocatalyst activity of layered δ-MnO₂ phase than α-MnO₂ phase, the present multilayer δ-MnO₂–carbon hybrid nanosheets show a much superior electrocatalyst performance for Li–O₂ battery over the other MnO₂-based hybrid materials including α-MnO₂-containing ones, highlighting the remarkable merit of the present heterolayer hybridization strategy in exploring novel efficient electrocatalysts. The excellent electrocatalyst/electrode performances of hybrid nanosheets are attributable to the optimization of interfacial charge transfer, pore structure, enhanced electrocatalysis kinetics, and reversible formation/decomposition of discharged product during cycling in Li–O₂ batteries originated from their unique multilayer structure. The synthetic method developed in this study provides an effective protocol to explore diverse 2D multilayer hybrid nanosheets with synergistically-improved functionalities, emphasizing the crucial importance and novelty of the present research. Considering vast pools for exfoliated inorganic nanosheets like transition metal oxides, transition metal dichalcogenides, and layered double hydroxides with tailororable physicochemical properties as well as coating carbon/inorganic layers with various functionalities, there are new opportunities to develop various 2D multilayered hybrid nanosheets with excellent

Supporting information

Synthetic and characterization methods. Structural and resistance parameters determined by XPS and EIS analyses. HR-TEM, N₂ adsorption–desorption isotherms, and electrochemical performance results are given in Supporting Information.

Acknowledgments

This work was supported by the National Research Foundation of Korea (NRF) grant funded by the Korea government (MSIP) (NRF-2017R1A2A1A17069463, NRF-2017R1A2B3004383) and by the Korea government (MSIT) (NRF-2017R1A5A1015365). The experiments at PAL were supported in part by MOST and POSTECH.

Appendix A. Supplementary data

Supplementary material related to this article can be found, in the online version, at doi:<https://doi.org/10.1016/j.apcatb.2019.05.025>.

References

- S. Matthew, J. Song, Earth-abundant inorganic electrocatalysts and their nanostructures for energy conversion applications, *Energy Environ. Sci.* 7 (2014) 3519–3542.
- Z.K. Yang, C.-Z. Yuan, A.-W. Xu, Confined pyrolysis within a nanochannel to form a highly efficient single iron site catalyst for Zn–air batteries, *ACS Energy Lett.* 3 (2018) 2383–2389.
- X. Jin, S.-J. Shin, N. Kim, B. Kang, H. Piao, J.-H. Choy, H. Kim, S.-J. Hwang, Superior role of MXene nanosheet as hybridization matrix over graphene in enhancing interfacial electronic coupling and functionalities of metal oxide, *Nano Energy* 53 (2018) 841–848.
- Y. Meng, W. Song, H. Huang, Z. Ren, S.-Y. Chen, S.L. Suib, Structure–property relationship of bifunctional MnO₂ nanostructures: highly efficient, ultra-stable electrochemical water oxidation and oxygen reduction reaction catalysts identified in alkaline media, *J. Am. Chem. Soc.* 136 (2014) 11452–11464.
- K. Song, E. Cho, Y.-M. Kang, Morphology and active-site engineering for stable round-trip efficiency Li–O₂ batteries: a search for the most active catalytic site in Co₃O₄, *ACS Catal.* 5 (2015) 5116–5122.
- J. Park, H. Kim, K. Jin, B.J. Lee, Y.-S. Park, H. Kim, I. Park, K.D. Yang, H.-Y. Jeong, J. Kim, K.T. Hong, H.W. Jang, K. Kang, K.T. Nam, A new water oxidation catalyst: lithium manganese pyrophosphate with tunable Mn valency, *J. Am. Chem. Soc.* 136 (2014) 4201–4211.
- H.S. Jeon, S.J. Ahn, M.S. Jee, S.S. Yoon, Y.J. Hwang, B.K. Min, Water oxidation by manganese oxide electrocatalytic films synthesized by chemical solution deposition method, *J. Electrochem. Soc.* 163 (2016) F3113–F3118.
- Z. Zhang, J. Liu, J. Gu, L. Su, L. Cheng, An overview of metal oxide materials as electrocatalysts and supports for polymer electrolyte fuel cells, *energy environ. Sci.* 7 (2014) 2535–2558.
- M.S. Islam, M. Kim, X. Jin, S.M. Oh, N.-S. Lee, H. Kim, S.-J. Hwang, Bifunctional 2D superlattice electrocatalysts of layered double hydroxide–transition metal dichalcogenide, *ACS Energy Lett.* 3 (2018) 952–960.
- H. Jin, J. Wang, D. Su, Z. Wei, Z. Pang, Y. Wang, In situ cobalt–cobalt oxide/n-doped carbon hybrids as superior bifunctional electrocatalysts for hydrogen and oxygen evolution, *J. Am. Chem. Soc.* 137 (2015) 2688–2694.
- C. Tan, X. Cao, X.-J. Wu, Q. He, J. Yang, X. Zhang, J. Chen, W. Zhao, S. Han, G.-H. Nam, M. Sindoro, H. Zhang, Recent advances in ultrathin two-dimensional nanomaterials, *Chem. Rev.* 117 (2017) 6225–6331.
- C. Li, Y. Yu, M. Chi, L. Cao, Epitaxial nanosheet–nanowire heterostructures, *Nano Lett.* 13 (2013) 948–953.
- Y. Huang, X. Huang, J. Lian, D. Xu, L. Wang, X. Zhang, Self-assembly of ultrathin porous NiO nanosheets/graphene hierarchical structure for high-capacity and high-rate lithium storage, *J. Mater. Chem. B* 22 (2012) 2844–2847.
- I.Y. Kim, S. Park, H. Kim, R.S. Ruoff, S.-J. Hwang, Strongly-coupled freestanding hybrid films of graphene and layered titanate nanosheets: an effective way to tailor the physicochemical and antibacterial properties of graphene film, *Adv. Funct. Mater.* 24 (2014) 2288–2294.
- S. Lee, X. Jin, I.Y. Kim, T.-H. Gu, J.-W. Choi, S. Nahm, S.J. Hwang, Superior additive of exfoliated RuO₂ nanosheet for optimizing the electrode performance of metal oxide over graphene, *J. Phys. Chem. C* 120 (2016) 11786–11796.
- S. Li, C. Xin, X. Liu, Y. Feng, Y. Liu, J. Zheng, F. Liu, Q. Huang, Y. Qiu, J. He, J. Luo, F. Pan, 2D hetero-nanosheets to enable ultralow thermal conductivity by all scale phonon scattering for highly thermoelectric performance, *Nano Energy* 30 (2016) 780–789.
- Z.-M. Wang, W. Wang, N. Coombs, N. Soheilinia, G.A. Ozin, Graphene oxide–Periodic mesoporous silica sandwich nanocomposites with vertically oriented channels, *ACS Nano* 4 (2010) 7437–7450.
- L. Shan, T. Bian, B. Zhang, D. Zhang, L.-Z. Wu, C.-H. Tung, Y. Yin, T. Zhang, Graphene-supported ultrafine metal nanoparticles encapsulated by mesoporous silica: robust catalysts for oxidation and reduction reactions, *Angew. Chem. Int. Ed.* 53 (2014) 250–254.
- Y. Fang, Y. Lv, F. Gong, A.A. Elzatahy, G. Zheng, D. Zhao, Synthesis of 2D-mesoporous-Carbon/MoS₂ heterostructures with well-defined interfaces for high-performance lithium-ion batteries, *Adv. Mater.* 28 (2016) 9385–9390.
- K. Möller, J. Kobler, T. Bein, Colloidal suspensions of nanometer sized mesoporous silica, *Adv. Funct. Mater.* 17 (2007) 605–612.
- J. Ahn, K.J. Lee, W. Bak, J.-J. Kim, J.-K. Lee, W.C. Yoo, Y.-E. Sung, Elucidating relationships between structural properties of nanoporous carbonaceous shells and electrochemical performances of Si@Carbon anodes for lithium-ion batteries, *J. Phys. Chem. C* 119 (2015) 10255–10265.
- J. Xiao, D. Mei, X. Li, W. Xu, D. Wang, G.L. Graff, W.D. Bennett, Z. Nie, L.V. Saraf, I.A. Aksay, J. Liu, J.-G. Zhang, Hierarchically porous graphene as a lithium-air battery electrode, *Nano Lett.* 11 (2011) 5071–5078.
- H. Zhou, S. Zhu, M. Hibino, I. Honma, M. Ichihara, Lithium storage in ordered mesoporous carbon (CMK-3) with high reversible specific energy capacity and good cycling performance, *Adv. Mater.* 15 (2003) 2107–2111.
- R.L. Liu, D.Q. Wu, X. Feng, L.K. Müllen, Nitrogen-doped ordered mesoporous graphitic arrays with high electrocatalytic activity for oxygen reduction, *Angew. Chem. Int. Ed.* 49 (2010) 2565–2569.
- H.A. Becerril, J. Mao, Z.F. Liu, R.M. Stoltenberg, Z.N. Bao, Y.S. Chen, Evaluation of solution-processed reduced graphene oxide films as transparent conductors, *ACS Nano* 3 (2008) 463–470.
- B. Sjögren, S. Svensson, A. Naves de Brito, N. Correia, M.P. Keane, C. Enkvist, S. Lunell, The C 1s core shake-up spectra of alkene molecules: an experimental and theoretical study, *J. Chem. Phys.* 96 (1992) 6389.
- H. Yamaguchi, A. Yamada, H. Uwe, Jahn–Teller transition of LiMn₂O₄ studied by X-Ray-Absorption spectroscopy, *Phys. Rev. B* 58 (1998) 8–11.
- Y. Gorlin, T.F. Jaramillo, A bifunctional nonprecious metal catalyst for oxygen reduction and water oxidation, *J. Am. Chem. Soc.* 132 (2010) 13612–13614.
- K. Kinoshita, *Electrochemical oxygen technology*, Wiley-Interscience, New York,

1992.

[30] A. Yu, H.W. Park, A. Davies, D.C. Higgins, Z. Chen, X. Xiao, Free-standing layer-by-layer hybrid thin film of graphene–MnO₂ nanotube as anode for lithium ion batteries, *J. Phys. Chem. Lett.* 2 (2011) 1855–1860.

[31] B.D. Mohapatra, S.P. Mantry, N. Behera, B. Behera, S. Rath, K.S.K. Baradwaj, Stimulation of electrocatalytic oxygen reduction activity on nitrogen doped graphene through noncovalent molecular functionalisation, *Chem. Commun. (Camb.)* 52 (2016) 10385–10388.

[32] R.K. Gautam, H. Bhattacharjee, S.V. Mohan, A. Verma, Nitrogen doped graphene supported α -MnO₂ nanorods for efficient ORR in a microbial fuel cell, *RSC Adv.* 6 (2016) 110091–110101.

[33] K. Song, J. Jung, Y.-U. Heo, Y.C. Lee, K. Cho, Y.-M. Kang, α -MnO₂ nanowire catalysts with ultra-high capacity and extremely low overpotential in lithium–air batteries through tailored surface arrangement, *Phys. Chem. Chem. Phys.* 15 (2013) 20075–20079.

[34] S. Liu, G. Wang, F. Tu, J. Xie, H.Y. Yang, S. Zhang, T. Zhu, G. Cao, X. Zhao, Au-nanocrystals-decorated α -MnO₂ as an efficient catalytic cathode for high-performance Li–O₂ batteries, *Nanoscale* 7 (2015) 9589–9596.

[35] P. Zhang, M. He, S. Xub, X. Yan, The controlled growth of porous α -MnO₂ nanosheets on carbon fibers as a bifunctional catalyst for rechargeable lithium–oxygen batteries, *J. Mater. Chem. A Mater. Energy Sustain.* 3 (2015) 10811–10818.

[36] S. Liu, Y. Zhu, J. Xie, Y. Huo, H.Y. Yang, T. Zhu, G. Cao, X. Zhao, S. Zhang, Direct growth of flower-like α -MnO₂ on three-dimensional graphene for high-performance rechargeable Li–O₂ batteries, *Adv. Energy Mater.* 4 (2014) 1301960.

[37] J. Wang, L.L. Liu, C.M. Subramanyam, S.L. Chou, H.K. Liu, J.Z. Wang, A microwave autoclave synthesized 8-MnO₂/graphene composite as a cathode material for lithium–oxygen batteries, *J. Appl. Electrochem.* 46 (2016) 869–878.

[38] M. Salehi, Z. Shariatinia, Synthesis of star-like MnO₂–CeO₂/CNT composite as an efficient cathode catalyst applied in lithium–oxygen batteries, *Electrochim. Acta* 222 (2016) 821–829.

[39] C. Cao, Z.Y. Lan, Y.C. Yan, H. Cheng, B. Pan, J. Xie, Y.H. Lu, H. Zhang, S.C. Zhang, G.S. Cao, X.B. Zhao, Mechanistic insight into the synergistic catalytic effect of Pd and MnO₂ for high-performance Li–O₂ cells, *Energy Storage Mater.* 12 (2018) 8–16.

[40] S.R. Cai, M.S. Zheng, X.D. Lin, M. Lei, R.M. Yuan, Q.F. Dong, A synergistic catalytic mechanism for oxygen evolution reaction in aprotic Li–O₂ battery, *ACS Catal.* 8 (2018) 7983–7990.

[41] K. Adpakpang, S.M. Oh, D.A. Agyeman, X.Y. Jin, N. Jarulertwathana, I.Y. Kim, T. Sarakonsri, Y.M. Kang, S.-J. Hwang, Holey 2D nanosheets of low-valent manganese oxides with an excellent oxygen catalytic activity and a high functionality as a catalyst for Li–O₂ batteries, *Adv. Funct. Mater.* 28 (2018) 1707106.

[42] Y.J. Lee, D.H. Kim, T.G. Kang, Y. Ko, K. Kang, Y.J. Lee, Bifunctional MnO₂-coated Co₃O₄ hetero-structured catalysts for reversible Li–O₂ batteries, *Chem. Mater.* 29 (2017) 10542–10550.

[43] P. Zhang, S.F. Zhang, M. He, J.W. Lang, A.M. Ren, S. Xu, X.B. Yan, Realizing the embedded growth of large Li₂O₂ aggregations by matching different metal oxides for high-capacity and high-rate lithium oxygen batteries, *Adv. Sci.* 4 (2017) 1700172.

[44] Y. Yu, B. Zhang, Y.-B. He, Z.-D. Huang, S.-W. Oh, J.-K. Kim, Mechanisms of capacity degradation in reduced graphene oxide/ α -MnO₂ nanorod composite cathodes of Li-air batteries, *J. Mater. Chem. A Mater. Energy Sustain.* 1 (2013) 1163–1170.

[45] Y. Cao, Z. Wei, J. He, J. Zang, Q. Zhang, M. Zheng, Q. Dong, α -MnO₂ nanorods grown in situ on graphene as catalysts for Li–O₂ batteries with excellent electrochemical performance, *Energy Environ. Sci.* 5 (2012) 9765–9768.

[46] Y. Qin, J. Lu, P. Du, Z. Chen, Y. Ren, T. Wu, J.T. Miller, J. Wen, D.J. Miller, Z. Zhang, K. Amine, In situ fabrication of porous-carbon-supported α -MnO₂ nanorods at room temperature: application for rechargeable Li–O₂ batteries, *Energy Environ. Sci.* 6 (2013) 519–531.

[47] A. Zahoor, M. Christy, H. Jang, K.S. Nahm, Y.S. Lee, Increasing the reversibility of Li–O₂ batteries with caterpillar structured α -MnO₂/N-GNF bifunctional electrocatalysts, *Electrochim. Acta* 157 (2015) 299–306.

[48] Q.C. Liu, J.J. Xu, Z.W. Chang, X.B. Zhang, Direct electrodeposition of cobalt oxide nanosheets on carbon paper as free-standing cathode for Li–O₂ battery, *J. Mater. Chem. A Mater. Energy Sustain.* 2 (2014) 6081–6085.

[49] J. Wang, L.L. Liu, C.M. Subramanyam, S.L. Chou, H.K. Liu, J.Z. Wang, A microwave autoclave synthesized 8-MnO₂/graphene composite as a cathode material for lithium–oxygen batteries, *J. Appl. Electrochem.* 46 (2016) 869–878.

[50] X. Zhu, P. Zhang, S. Xu, X. Yan, Q. Xue, Free-standing three-dimensional Graphene/Manganese oxide hybrids as binder-free electrode materials for energy storage applications, *ACS Appl. Mater. Interfaces* 6 (2014) 11665–11674.

[51] I. Bardenhagen, M. Fenske, D. Fenske, A. Wittstock, M. Bäumer, Distribution of discharge products inside of the Lithium/Oxygen battery cathode, *J. Power Sources* 299 (2015) 162–169.